An Experimental and Computational Study of the Thermal Oxidation of C_6H_5NO by NO_2

J. Park, Y. M. Choi, I. V. Dyakov, and M. C. Lin*

Department of Chemistry, Emory University, Atlanta, Georgia 30322

Received: September 14, 2001; In Final Form: January 7, 2002

The kinetics and mechanism for the thermal oxidation of nitrosobenzene by nitrogen dioxide have been studied experimentally by pyrolysis/Fourier transform infrared spectrometry and computationally by hybrid density functional theory calculations. The experimental data measured in the temperature range 373−473 K gave rise to the bimolecular rate constant for the direct O-exchange reaction, $C_6H_5NO + NO_2 \rightarrow C_6H_5NO_2 + NO$, $k_1 = (9.62 \pm 0.35) \times 10^{10} \exp[-(6500 \pm 144)/T]$ cm^3 mol^{-1} s^{-1}, which can be satisfactorily accounted for by the transition-state theory with the energy barrier, $E_1^0 = 10.0 \pm 0.3$ kcal mol^{-1} at 0 K.

I. Introduction

The possibility of the thermal oxidation of nitrosomethane by nitrogen dioxide to nitromethane in the gas phase, $CH_3NO + NO_2 \rightarrow CH_3NO_2 + NO$, was first suggested by Phillips and Shaw.[1] Cooper et al.[2] confirmed the reaction in their study of the $CH_3 + NO_2$ reaction in the presence of NO in the temperature range 323−455 K. They detected excess yields of CH_3NO_2, which could not be accounted for by the association of CH_3 with NO_2 alone. An approximate rate constant for the reaction was obtained by kinetic modeling, $k \approx 10^9 \exp(-5030/T)$ cm^3 mol^{-1} s^{-1}, with about 10 kcal mol^{-1} activation energy.

In a recent study of the thermal decomposition of C_6H_5NO in the presence of NO_2, we noted the formation of $C_6H_5NO_2$ in a long-standing, highly diluted mixture of C_6H_5NO and NO_2 at room temperature, attributable to the occurrence of the analogous redox reaction mentioned above. To confirm such a possibility, we have measured the decay of C_6H_5NO and the formation of $C_6H_5NO_2$ and NO by Fourier transform infrared (FTIR) spectrometry in the temperature range 373−473 K under atmospheric Ar-pressure conditions.

To further substantiate that nitrobenzene was indeed formed by the direct oxidation reaction,

$$C_6H_5NO + NO_2 \rightarrow C_6H_5NO_2 + NO \qquad (1)$$

we have performed a quantum chemical calculation using the hybrid density functional (B3LYP) method. Such a direct displacement transition state was indeed found, and the predicted transition-state parameters were employed for calculation of the bimolecular rate constant, k_1, for comparison with experimental data. Both experimental and theoretical results are presented herein.

II. Experimental Procedure

The thermal reaction of C_6H_5NO with NO_2 was studied in a spherical quartz reactor of 270 cm^3 in volume enclosed in a temperature-controlled cylindrical furnace. The temperature was controlled and held within ±0.5 K using an Omega CN-9000 solid-state temperature controller. A K-type thermocouple was placed at the center of the reactor in a small quartz tube. The detailed experimental procedure of the pyrolysis/FTIR spectrometric technique can be found in our earlier studies.[3,4]

For kinetic measurements, the reactor was filled to an appropriate pressure with a mixture of NO_2 and Ar, to which an Ar-diluted mixture of C_6H_5NO was added up to 760 (±0.5) Torr in the temperature range 393−473 K. Pyrolyzed or unpyrolyzed reference samples were expanded into the absorp-

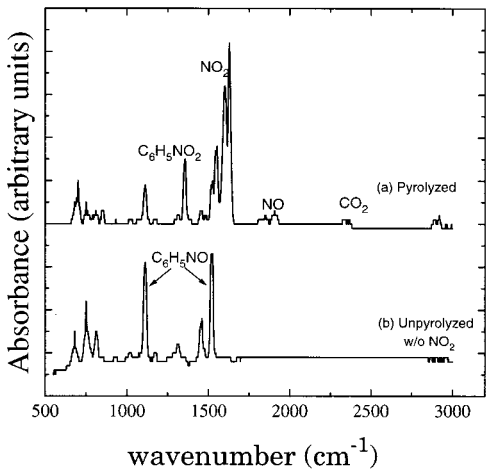

Figure 1. Typical FTIR spectra of pyrolyzed and unpyrolyzed mixtures of $C_6H_5NO/NO_2/Ar$.

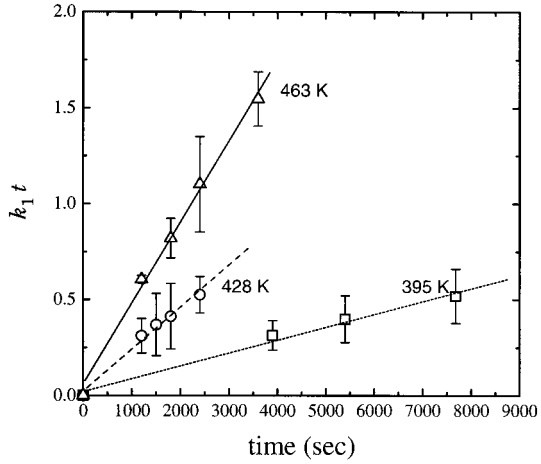

Figure 2. Second-order kinetics plot according to eq 2.

* To whom correspondence should be addressed. E-mail: chemmcl@emory.edu.

10.1021/jp0135353 CCC: $22.00
Published on Web 03/05/2002

TABLE 1: Summary of the Experimental Conditions and Rate Constant for the Reaction of C_6H_5NO with NO_2 at Different Temperatures[a]

T, K	$[C_6H_5NO]_0$	$[NO_2]_0$	k_{bim}	k_{mod}
373	2.78	3.27	0.28 ± 0.05	0.30 ± 0.04
395	2.62	3.12	0.67 ± 0.20	0.67 ± 0.06
418	2.27	2.62	1.33 ± 0.87	1.62 ± 0.33
428	2.22	2.56	2.32 ± 0.70	2.66 ± 0.39
438	2.17	2.50	3.69 ± 0.95	3.39 ± 0.20
443	2.26	2.48	2.73 ± 0.78	2.92 ± 0.50
458	2.08	2.39	5.66 ± 0.95	6.02 ± 0.42
463	2.16	2.37	5.67 ± 0.89	5.39 ± 0.72
473	2.11	2.32	8.99 ± 0.75	7.88 ± 1.12
473	2.16	1.65	10.8 ± 2.30	10.4 ± 0.80

[a] The concentrations are given in units of 10^{-8} mol cm^{-3}, and rate constants are given in units of 10^4 cm^3 mol^{-1} sec^{-1}. The total pressure of all experiments was 1 atm with the bath gas of argon.

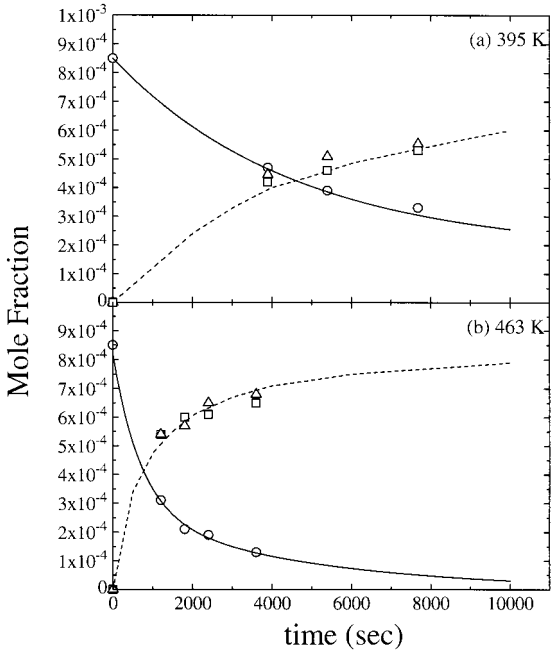

Figure 3. The concentration profiles of the reactants and products measured in the pyrolysis of $C_6H_5NO/NO_2/Ar$ mixture as functions of time: (○) C_6H_5NO; (□) NO; (△) $C_6H_5NO_2$. Solid curves represent modeled results of C_6H_5NO; dashed curves represent modeled results of $C_6H_5NO_2$ and NO.

tion cell inside the FTIR spectrometer (Mattson Instruments, Polaris) and converted to absolute concentrations. The absolute concentrations of the reactants and products were determined by using standard calibration curves plotted in concentration vs absorbance peak height measured at 1113.0 cm^{-1} for C_6H_5NO, 1630.0 cm^{-1} for NO_2, 1905.8 cm^{-1} for NO, and 1358.0 cm^{-1} for $C_6H_5NO_2$. Typical error in the determination of

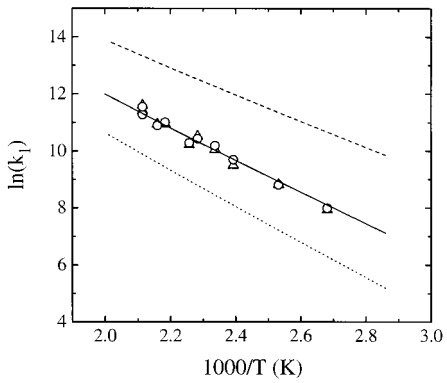

Figure 4. Arrhenius plot for k_1: (△) result by eq 2; (○) result by kinetic modeling; solid line, predicted rate constant with E_a = 10.0 kcal mol^{-1}; dashed and dotted lines, predicted rate constants with E_a = 8.1 kcal mol^{-1} at the B3LYP/cc-pvDZ level and 11.3 kcal mol^{-1} at the B3LYP/aug-cc-PVTZ//B3LYP/cc-PVDZ level, respectively.

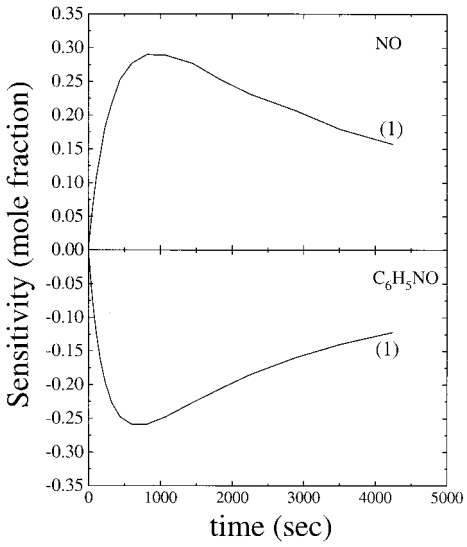

Figure 5. Sensitivity analyses for C_6H_5NO and NO at 473 K.

absorbance peak heights is 5%. The pressures of the samples after expansion were approximately 320 Torr. To minimize the effect of pressure broadening, the pressure of calibration mixtures containing varying amounts of the reactants and products was maintained at 320 ± 10 Torr. Figure 1 shows a typical set of FTIR spectra obtained before and after the pyrolysis of a mixture containing C_6H_5NO and NO_2.

The reaction mixtures were prepared with the following initial concentrations: 0.081−0.089% of C_6H_5NO and 0.064−0.090% of NO_2 with argon (99.9995%, Specialty Gases) dilution separately made in different glass bulbs. The NO_2 (Matheson) and NO (Matheson) were purified by the standard trap-to-trap

TABLE 2: Reaction Mechanism and Rate Constants[a] Employed for Kinetic Modeling of the $C_6H_5NO + NO_2$ System

	reaction	A	n	E_a	ref[b]
1	$C_6H_5NO + NO_2 \rightarrow C_6H_5NO_2 + NO$	9.62×10^{17}	0.0	12 900	this work
2	$C_6H_5NO = C_6H_5 + NO$	1.42×10^{17}	0.0	55 060	
3	$C_6H_5 + NO_2 \rightarrow C_6H_5NO_2$	2.69×10^{12}	0.0	−860	*c*
4	$C_6H_5 + C_6H_5 = C_{12}H_{10}$	1.39×10^{13}	0.0	111	
5	$C_6H_5 + C_6H_5NO \rightarrow C_{12}H_{10} + NO$	5.00×10^{12}	0.0	4500	
6	$C_6H_5 + C_6H_5NO \rightarrow C_{12}H_{10}NO$	4.90×10^{12}	0.0	−68	
7	$C_{12}H_{10}NO \rightarrow C_6H_5NO + C_6H_5$	5.00×10^{14}	0.0	45 000	
8	$C_{12}H_{10}NO + C_6H_5 \rightarrow C_{12}H_{10}N + C_6H_5O$	1.00×10^{13}	0.0	0	
9	$C_{12}H_{10}N + NO \rightarrow C_{12}H_{10}NNO$	1.00×10^{13}	0.0	0	

[a] Rate constants, defined by $k = AT^n \exp(-E_a/(RT))$, are given in units of cm^3, mol, and s; E_a is in units of cal mol^{-1}. [b] The mechanism and associated kinetics are taken from ref 18. [c] Assumed to be the same as $C_6H_5 + NO$ (see ref 18).

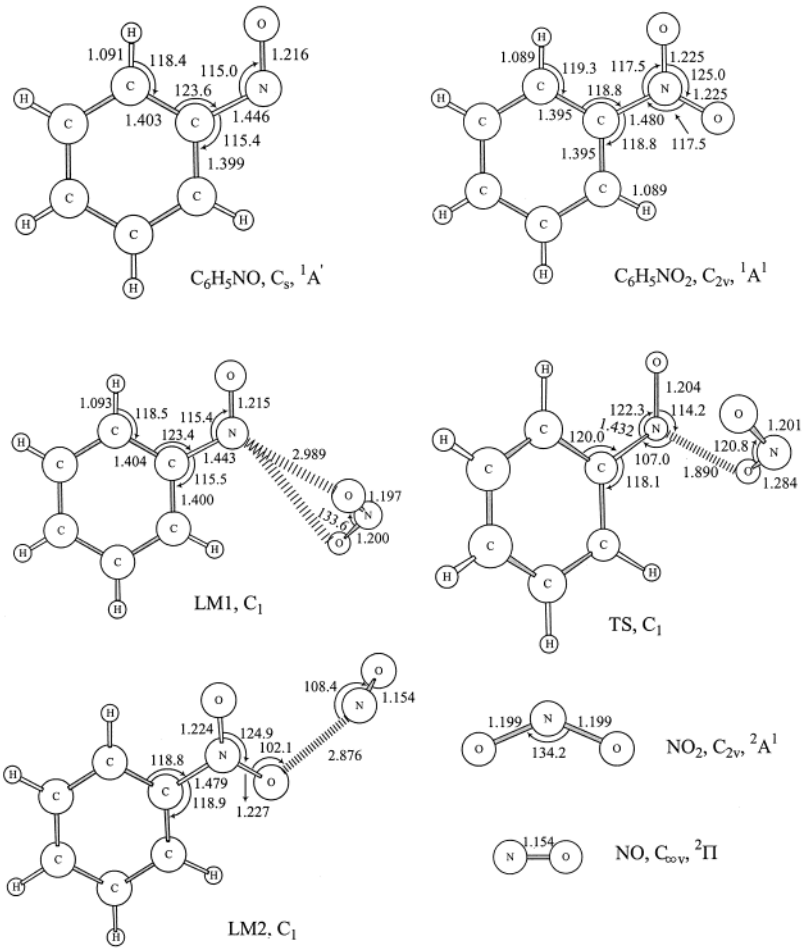

Figure 6. Optimized structures of the reactants, transition state, intermediates, and products for the $C_6H_5NO + NO_2 \rightarrow C_6H_5NO_2 + NO$ reaction at the B3LYP/cc-PVDZ level of theory. Bond lengths are in Å, and bond angles are in deg.

distillation using appropriate slush baths. C_6H_5NO (Aldrich) was purified by recrystallization at 273 K using C_2H_5OH as solvent, followed by extensive pumping at the same temperature to remove residual solvent.

III. Computational Methods

The hybrid density functional B3LYP method[5,6] with a correlation-consistent basis set (cc-PVDZ)[7,8] has been employed to optimize all of the structures of the reactants, intermediates, transition state, and products with the Gaussian 98 program.[9] From the equilibrium geometries, moments of inertia and harmonic vibrational frequencies were calculated at the same level of theory. For the transition-state search, the synchronous transit-guided quasi-Newton (STQN) method[10,11] with the QST2 option for optimizations has been employed, and the intrinsic reaction coordinate (IRC) method[12] and normal-mode analysis[13] have been utilized to validate the connection of the transition state with the reactants and products.

All of the stationary points were found by using the *tight* option[9] to improve accuracy and verified by the number of imaginary frequencies (N_{img}); that is, $N_{img} = 1$ for transition states and $N_{img} = 0$ for stable molecules. In this study, all of the energies include zero-point energy (ZPE) corrections using the computed frequencies. Also, single-point energies have been calculated at B3LYP/aug-cc-PVTZ using the geometry computed at the B3LYP/cc-PVDZ level of theory.

IV. Results and Discussion

A. Kinetic Data Analysis. Kinetic measurements have been performed at different temperatures with varying time intervals. The rate constant for the bimolecular reaction of C_6H_5NO with NO_2 can be effectively evaluated with the second-order rate law and kinetic modeling, which also helps to substantiate the former and the fact that secondary radical processes contribute negligibly to the measured kinetic data under the low-temperature conditions employed.

With the assumption that reaction 1 takes place exclusively by the bimolecular O-exchange process, k_1 can be calculated with the instantaneous concentrations of the reactants, [C_6H_5-NO] and [NO_2], and those of the products, [$C_6H_5NO_2$] and [NO], at time t measured by FTIR spectrometry according to the well-known rate law:[14]

$$\frac{\ln\left\{\frac{[C_6H_5NO]_0[NO_2]}{[C_6H_5NO][NO_2]_0}\right\}}{([NO_2]_0 - [C_6H_5NO]_0)} = k_1 t \qquad (2)$$

where $[X]_0$ denotes the initial concentration of species X. In eq 2, the values of [C_6H_5NO] and [NO_2] can be stoichiometrically replaced with those of [$C_6H_5NO_2$] and [NO], respectively. Figure 2 presents three typical second-order plots; the slopes of the plots give k_1. Table 1 lists the evaluated values of k_1 as k_{bim} and compares them with those evaluated by kinetic modeling, k_{mod}.

Kinetic modeling was carried out with the mechanism summarized in Table 2 using the SENKIN program[15] in conjunction with CHEMKIN thermochemical data.[16] Figure 3 shows some typical concentration profiles of both experimental

TABLE 3: Moments of Inertia (I_A, I_B, I_C) and Vibrational Frequencies of the Species Involved in the $C_6H_5NO + NO_2 = C_6H_5NO_2 + NO$ Reaction at the B3LYP/cc-PVDZ Level

molecules	I_i (10^{-40} g cm^2)	vibrational frequencies (cm^{-1})
C_6H_5NO	160.2 513.4 673.6	120, 250, 258, 422, 446, 481, 622, 681, 702, 787, 833, 875, 976, 1013, 1015, 1029, 1035, 1088, 1128, 1171, 1189, 1322, 1379, 1481, 1496, 1600, 1646, 1663, 3178, 3189, 3196, 3206, 3212
NO_2	3.5 64.8 68.3	758, 1406, 1722
$C_6H_5NO_2$	212.0 655.5 867.5	63, 172, 258, 397, 421, 451, 528, 622 694, 696, 719, 811, 862, 867, 969, 1001, 1017, 1024, 1042, 1091, 1122, 1172, 1185, 1318, 1375, 1397, 1485, 1505, 1625, 1640, 1675, 3184, 3197, 3206, 3238, 3238
NO	0.0 16.5 16.5	1994
TS	404.1 1063.9 1172.4	239i, 44, 60, 128, 158, 191, 263, 369, 400, 419, 480, 532 621, 645, 695, 775, 814, 830, 854, 951, 995, 1008, 1016, 1018, 1041, 1098, 1138, 1172, 1194, 1326, 1370, 1481, 1499, 1563, 1622, 1639, 1661, 3184, 3196, 3206, 3224, 3225

TABLE 4: Relative Energies in kcal mol^{-1} of the Reactants, Transition State, Intermediates, and Products for the $C_6H_5NO + NO_2 \rightarrow C_6H_5NO_2 + NO$ Reaction Calculated at the B3LYP/cc-PVDZ and B3LYP/aug-cc-PVTZ Levels of Theory

species	ZPE	B3LYP/cc-PVDZ	B3LYP/aug-cc-PVTZ
$C_6H_5NO + NO_2$	66.6	0.0[a]	0.0[b]
$C_6H_5NO \cdot NO_2$	67.2	−2.4	0.2[c]
TS	67.3	8.1	11.3
$C_6H_5NO_2 \cdot NO$	67.9	−16.4	−15.1[c]
$C_6H_5NO_2 + NO$	67.6	−15.2	−15.5

[a] Total energy in hartrees is −566.551 995. [b] Total energy in hartrees is −566.727 985. [c] The reason the relative energies are higher than those of reactants and products may be the error of the single-point energy calculations.

and modeled results of C_6H_5NO, $C_6H_5NO_2$, and NO vs time. In the modeling, the value of k_1 was adjusted to fit the experimental data at different time intervals and the averaged value was used in the final calculation. As shown in Table 1, the modeled value, k_{mod}, at each temperature agrees closely with k_{bim} calculated by eq 2. Figure 4 summarizes both sets of results graphically in an Arrhenius plot. A weighted least-squares analysis[17] of the two sets of data gave rise to

$$k_1 = (9.62 \pm 0.35) \times 10^{10} \exp[-(6500 \pm 144)/T] \text{ cm}^3 \text{ mol}^{-1} \text{ s}^{-1} \quad (3)$$

The good agreement between the results obtained by eq 2 and those obtained by kinetic modeling including potential secondary radical reactions as listed in Table 2 clearly suggests that the secondary reactions do not occur to any significant extent. At the highest temperature employed, 473 K, the half-life of C_6H_5NO, which dissociates more effectively than NO_2 does, is calculated to be $\sim 10^8$ s on the basis of the rate constant for its unimolecular decomposition reaction recently determined by FTIR spectrometry in our laboratory.[18] The result of a sensitivity analysis at 473 K for C_6H_5NO and NO (Figure 5) clearly shows that only reaction 1 is responsible for the decay of C_6H_5NO and the formation of NO.

B. Confirmation of the Mechanism by Quantum Calculation. The mechanism of the reaction has been confirmed by calculation with the B3LYP/cc-PVDZ method. The optimized structures and molecular parameters of the reactants, transition state, intermediates, and products are presented in Figure 6 and Table 3, respectively. Additional single-point energies have been computed at the B3LYP/aug-cc-PVTZ level, using the geometry optimized at B3LYP/cc-PVDZ, for comparison. The two sets of relative energies are summarized in Table 4. The schematic energy diagram of this reaction using the energies predicted at the B3LYP/cc-PVDZ level is illustrated in Figure 7.

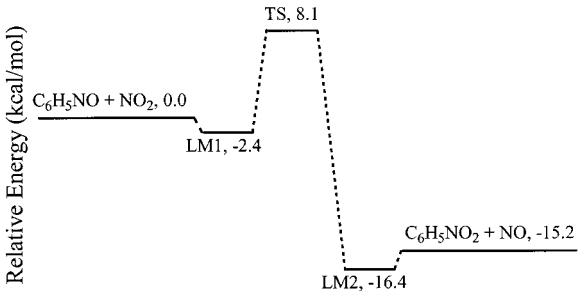

Figure 7. Schematic energy diagram for the $C_6H_5NO + NO_2 \rightarrow C_6H_5NO_2 + NO$ reaction calculated at the B3LYP/cc-PVDZ level of theory.

Mechanistically, the oxidation of C_6H_5NO by NO_2 was found to take place via a local minimum (LM) of the reactants, the transition state, and the LM of the products, $C_6H_5NO_2$ and NO:

$$C_6H_5NO + NO_2 \rightarrow LM1 \rightarrow TS^{\ddagger} \rightarrow LM2 \rightarrow C_6H_5NO_2 + NO$$

where "‡" represents the transition state. The local minimum of the reactants, LM1, found by IRC analysis, has a binding energy of 2.4 kcal mol^{-1}. The bond lengths between the O atoms of NO_2 and the N atom of C_6H_5NO are 2.989 and 3.189 Å, respectively. At the transition state, the forming N−O bond becomes 1.890 Å with the departing NO group lying above the ONCC frame. The barrier for the reaction was predicted to be 8.1 kcal mol^{-1} at the B3LYP/cc-PVDZ level and 11.3 kcal mol^{-1} at the B3LYP/aug-cc-PVTZ//B3LYP/cc-PVDZ level (see Table 4). After overcoming the reaction barrier, the reaction first forms the local minimum of the products, LM2, with the exothermicity of 16.4 kcal mol^{-1} at B3LYP/cc-PVDZ and 15.1 kcal mol^{-1} at B3LYP/aug-cc-PVTZ, and the overall exothermicity of 15.2 and 15.5 kcal mol^{-1}, respectively. The binding energy of LM2 is negligibly small ($\sim$0) within the reliability of the approximate B3LYP method.

Rate Constant Calculation. The predicted transition-state parameters and energies presented above were utilized to calculate the bimolecular rate constant for the O-exchange reaction using the conventional transition-state theory.[14] As the binding energy of LM1 is small compared with the reaction barrier, the effect of LM2 to the kinetics is evidently insignificant.

The predicted rate constants based on the two values of the barrier, 8.1 and 11.3 kcal mol^{-1}, are included in Figure 4 for comparison with experimental data. The rate constant predicted with the 8.1 kcal mol^{-1} barrier obtained at the B3LYP//cc-PVDZ level of theory is higher than the experimental result by a factor of 10 at the middle temperature studied (428 K), whereas the larger barrier (11.3 kcal mol^{-1}) underpredicted the rate constant by a factor of 5 at the same temperature.

To quantitatively account for the experimental result, the reaction barrier should lie in the vicinity of 10.0 ± 0.3 kcal mol^{-1}, which is within the uncertainty of the approximate hybrid density functional theory with a computationally affordable size of basis set.

V. Conclusion

The rate constant for the oxidation of nitrosobenzene by nitrogen dioxide has been measured in the temperature range 373−473 K. The rates of C_6H_5NO decay and the formation of $C_6H_5NO_2$ and NO measured by FTIR spectrometry can bequantitatively accounted for by the direct O-exchange reaction,

$$C_6H_5NO + NO_2 \rightarrow C_6H_5NO_2 + NO \qquad (1)$$

with the rate constant $k_1 = (9.62 \pm 0.35) \times 10^{10} \exp[-(6500 \pm 144)/T]$ cm^3 mol^{-1} s^{-1}. The mechanism of this metathetical process was confirmed by a quantum chemical calculation using the hybrid density functional theory, and the rate constant can be accounted for by the transition-state theory based on the predicted transition-state parameters with the energy barrier $E_1 = 10.0 \pm 0.3$ kcal mol^{-1} at 0 K.

Acknowledgment. The authors are grateful for the support of this work from the Basic Energy Sciences, Department of Energy, under Contract No. DE-FG02-97-ER14784.

References and Notes

(1) Phyllips, L.; Shaw, R. *10th Symposium (International) on Combustion*; The Combustion Institute: 1965; p 453.

(2) Cooper, S. C.; Umstead, M. E.; Kolby, K.; Lin, M. C. *J. Energ. Mater*. **1989**, *7*, 55.

(3) Aldridge, K. H.; Liu, X.; Lin, M. C.; Melius, C. F. *Int. J. Chem. Kinet.* **1991**, *23*, 947.

(4) Park, J.; Giles, N. D.; Moore, J.; Lin, M. C. *J. Phys. Chem. A* **1998**, *102*, 10098.

(5) (a) Becke, A. D. *J. Chem. Phys.* **1993**, *98*, 5648. (b) Becke, A. D. *J. Chem. Phys*. **1992**, *96*, 2155. (c) Becke, A. D. *J. Chem. Phys*. **1992**, *97*, 9173.

(6) Lee, C.; Yang, W.; Parr, R. G. *Phys. Rev. B* **1988**, *37*, 785.

(7) Woon, K. E.; Dunning, T. H., Jr. *J. Chem. Phys.*, **1993**, *98*, 1358; **1993**, *99*, 1914.

(8) Peterson, K. A.; Woon, D. E.; Dunning, T. H., Jr. *J. Chem. Phys.* **1994**, *100*, 7410.

(9) Frisch, M. J.; Trucks, G. W.; Schlegel, H. B.; Scuseria, G. E.; Robb, M. A.; Cheeseman, J. R.; Zakrzewski, V. G.; Montgomery, J. A., Jr.; Stratmann, R. E.; Burant, J. C.; Dapprich, S.; Millam, J. M.; Daniels, A. D.; Kudin, K. N.; Strain, M. C.; Farkas, O.; Tomasi, J.; Barone, V.; Cossi, M.; Cammi, R.; Mennucci, B.; Pomelli, C.; Adamo, C.; Clifford, S.; Ochterski, J.; Petersson, G. A.; Ayala, P. Y.; Cui, Q.; Morokuma, K.; Malick, D. K.; Rabuck, A. D.; Raghavachari, K.; Foresman, J. B.; Cioslowski, J.; Ortiz, J. V.; Stefanov, B. B.; Liu, G.; Liashenko, A.; Piskorz, P.; Komaromi, I.; Gomperts, R.; Martin, R. L.; Fox, D. J.; Keith, T.; Al-Laham, M. A.; Peng, C. Y.; Nanayakkara, A.; Gonzalez, C.; Challacombe, M.; Gill, P. M. W.; Johnson, B. G.; Chen, W.; Wong, M. W.; Andres, J. L.; Head-Gordon, M.; Replogle, E. S.; Pople, J. A. *Gaussian 98*, revision A.7; Gaussian, Inc.: Pittsburgh, PA, 1998.

(10) Peng, C.; Schlegel, H. B. *Isr. J. of Chem.* **1993**, *33*, 449.

(11) Peng, C.; Ayala, P. Y.; Schlegel, H. B.; Frisch, M. J. *J. Comput. Chem.* **1995**, *16*, 49.

(12) Gonzalez, C.; Schlegel, H. B. *J. Phys. Chem.* **1990**, *94*, 5523.

(13) Schaftenaar, G.; Noordik, J. H. *J. Comput.-Aided Mol. Des.* **2000**, *14*, 123.

(14) Laidler, K. J. *Chemical Kinetics*, 3rd ed.; Harper & Row: New York, 1987.

(15) Luts, A. E.; Lee, R. K.; Miller, J. A. *SENKIN: A FORTRAN Program for Predicting Homogeneous Gas-Phase Chemical Kinetics with Sensitivity Analysis*; Sandia National Laboratories Report No. SANDIA 87-8248; Sandia National Laboratories: 1988.

(16) Kee R. J.; Rupley, F. M.; Miller, J. A. *CHEMKIN−II: A FORTRAN chemical kinetic package for the analysis of has-phase chemical kinetics*; Sandia National Laboratories Report No. SANDIA 89-8009; Sandia National Laboratories: 1989.

(17) Cvetanovic, R. J.; Singleton, D. L.; Paraskevopoulos, G. *J. Phys. Chem*. **1979**, *83*, 50.

(18) Park, J.; Dyakov, I. V.; Mebel, A. M.; Lin, M. C. *J. Phys. Chem. A* **1997**, *101*, 6043.